Int. J. Electrochem. Sci., 17 **(2022)** Article Number: 220938, doi: 10.20964/2022.09.22

International Journal of
ELECTROCHEMICAL
SCIENCE
www.electrochemsci.org

Optimization of Alkali catalyzed hydrothermal carbonization of *Prosopis juliflora* woody biomass to biochar for copper and zinc adsorption and its application in supercapacitor

Mothil Sengottian[1], *Chitra Devi Venkatachalam*[2,*] *and Sathish Raam Ravichandran*[1]

[1] Department of Chemical Engineering, Kongu Engineering College, Perundurai, Erode, 638060, Tamil Nadu, India.
[2] Department of Food Technology, Kongu Engineering College, Perundurai, Erode, 638060, Tamil Nadu, India.
[*]E-mail: erchitrasuresh@gmail.com

Received: 3 May 2022 / *Accepted:* 26 June 2022 / *Published:* 7 August 2022

Although there are many possible routes for the desorption of pollutants, reuse and regeneration of the used adsorbents, the performance and the adsorption capacity is not restored fully and after several cycles again the adsorbent becomes a waste and finally an environmental concern. Thus an alternative route to handle this problem of disposal of used adsorbents, especially for heavy metal adsorption is needed. An attempt is made to use the biochar obtained from hydrothermal carbonization of *Prosopis juliflora* woody biomass using 5 wt% KOH alkali catalyst. Response surface methodology was used to obtain the optimum conditions for the hydrothermal carbonization process by changing the process parameters such as temperature (200-300°C), reaction time (15-45 min), and water loading in biomass (4-8 mL g^{-1}) to maximize mass yield and carbonization ratio. This biochar produced had good adsorption behaviour for Cu(II) and Zn(II) ions from its aqueous solutions with adsorption capacity of 217.39 mg g^{-1} and 149.25 mg g^{-1} respectively. The Copper and Zinc adsorbed hydrothermal carbonized biochar were further used as an active material for the supercapacitor and it was observed to possess good specific capacitance of 144.48 F g^{-1} and 104.56 F g^{-1} respectively. This study suggests a possible route to utilize the spent adsorbent as an energy storage material.

Keywords: Used adsorbent, Hydrothermal carbonization, Copper and Zinc adsorption, Supercapacitor material

1. INTRODUCTION

Supercapacitors act as the energy storage device that can store and release a large amount of energy compared to that of the conventional capacitors and can replace the batteries in near future. They have a higher power output with high cyclicality and long-term stability [1]. Carbon is the most

commonly used electrode material in forming the electrical double layer (EDL) of electrochemical capacitors and it is the most preferred material because of its less cost, commercial availability, and large specific surface area. The porous carbon is very much suitable for EDL formation as it has a lack of space charge with dynamic charge propagation and a good attraction of ions along the pore walls [2]. Biomass is a naturally abundant renewable resource and it acts as the source of porous carbon. Biomass is derived from both plants and animals which is rich in carbon and used in the production of heat and electricity. They include woody plant wastes, forest residues, wastes from farm crops, algae, industry wastes, and domestic wastes [3]. This biomass is converted into biochar employing thermochemical techniques such as pyrolysis, gasification, hydrothermal conversion (carbonization, liquefaction, gasification) and microwave treatment and the produced biochar has various applications in wastewater treatment, agricultural soil rejuvenation, syngas production, trans-esterification, etc., and its derived composites are used in electrochemical energy storage materials such as fuel cells, Supercapacitors, and batteries [4][5][6][7].

Hydrothermal carbonization (HTC) is the thermochemical conversion of biomass into a solid-phase rich in carbon called hydrochar or biochar, liquid phase i.e bio-oil and gaseous product rich in carbon-di-oxide at a temperature of 180-250℃ and pressure of 10-50 bar in the sub-critical water environment [8]. The hydrochar obtained from this process had less ash content compared to that obtained from torrefaction and it also resulted in a product with more a dispersed structure [9]. The hydrochar showed higher affinity towards dyes and heavy metal adsorption when compared with pyrolysis biochar and this is due to its ion exchange and complexation property, but commercially available activated carbon showed a higher adsorption capacity compared to the hydrochar [10][11]. The main advantage of the biochar obtained from hydrothermal carbonization is that it is very easily biodegradable with a half-life of 0.7-2.1 years compared to that of pyrolysis biochar which is 19.7-44.5 years; and also with biological post-treatment (i.e bio-composting), the minimal genotoxic and phytotoxic effect is neutralized [12][13]. A maximum yield of biochar of 67.94 % is achieved through hydrothermal carbonization and with enhanced residence time till 10 h showed significant change in morphology with better porosity [14].

Prosopis juliflora is one of the most dominant weeds of the world's 100 most invasive species and an intelligent survey on climatic suitability and projective modeling of biodiversity for India suggests that North, North-western, and Southern India are more vulnerable and has the most suitable condition for a wide spread of this weed and warns that these dangerous species need to be managed at the earliest [15]. A survey between January 2018 and July 2019 in the protected areas of three forest reserves—Guindy National Park, Point Calimere Wildlife Sanctuary, and Sathyamangalam Tiger Reserve for spatial detectability and density distribution of blackbuck *Antilope cervicapra* showed that the alien invasion of *Prosopis juliflora* has reduced the extent of grassland, habitat openness and grass productivity leading to poor living condition for the large herbivores in the region [16]. Another study at Point Calimere Wildlife Sanctuary on soil ecosystem showed that the presence of *Prosopis juliflora* has decreased the composition of the local plant community, soil microbial respiration, and enzyme activity in the soil and when removed indicated an increase in the ground vegetation cover along with 38% increase in the species richness [17]. Thus this invasive species can be effectively used as a source of biochar.

Prosopis juliflora has been used to produce solid biofuel by the following torrefaction at 230 to 310 ℃ for 30 min using bench-scale apparatus in an inert atmosphere giving high heat energy between 18.3 and 23.1 MJ kg^{-1} [18]. The alarming increase of the invasive species in Ethiopia has led to the carbonization of *Prosopis juliflora* at 300–600 ℃ and time 60–180 min which resulted in charcoal with a high heating value of 24.43 MJ kg^{-1} and has been used as carbon-neutral alternated fuel for cement factories [19]. It was observed that for *Prosopis juliflora* when carbonization temperature was increased from 400 to 700℃, the higher heating value (HHV) increased from 17.75 MJ kg^{-1} to 31.90 MJ kg^{-1} using an Improved Natural Draft Retort Reactor and this charcoal can be effectively used as fuel for smelting and barbecue [20]. The fast pyrolysis of *Prosopis juliflora* at 450 °C using a continuous Blade type reactor resulted in 50% bio-oil, 31% biochar, and the remaining 19% syngas, in which the bio-oil was tested for FTIR, TGA, GC-MS, ^{1}H NMR and ^{13}C NMR and reported to have organic compounds like phenolic, carbonyl, furfural and toluene which made it suitable to use as 35% diesel blend with performance slightly higher than that of the pure fossil diesel [21]. The subcritical hydrothermal treatment of *Prosopis juliflora* at 278 ℃, biomass to water loading of 20.13 % w/v, and time of 60 min in a 50 mL hydrothermal bomb resulted in a bio-oil containing long-chain alkanes, amines, carboxylic acids, ketones and phenols [22]. Thus thermochemical conversion of *Prosopis juliflora* can result in high energy-dense biochar and byproduct as bio-oil that can be used as a diesel blend.

Biomass-derived biochar from HTC has required porosity, surface properties, conductivity, and both physical and chemical stability to use it as an adsorbent and energy storage material. The use of catalysts during HTC enhances the degree of carbonization and provides better surface characteristics for the addition of key heteroatoms that significantly enhances the performance of the biochar [23][24]. The activated hydrothermal char produced from swine manure when used as an adsorbent to remove Pb(II) from aqueous solution exhibited a better adsorption capacity of 211.8 mg g^{-1} and also provided a good specific capacitance of 278 F g^{-1} at 0.5 A g^{-1} in 6 M KOH electrolyte when used as a supercapacitor material [25]. Waste termite biomass on carbonization at 900 °C, 9 h, and with a 3:1 KOH catalyst resulted in an activated carbon electrode having high specific capacitance of 91.76 F g^{-1} at 0.5 A g^{-1} in 1 M H_2SO_4 and 62.35 F g^{-1} at 0.5 A g^{-1} in 1 M ionic liquid as electrolyte [26]. The activated carbon synthesized from oil palm kernel shell was pyrolyzed and KOH activated was studied for electrochemical performance in three different aqueous electrolytes 1 M H_2SO_4, 1 M Na_2SO_4, and 6 M KOH, and produced a potential difference of 1.0 V, 1.2 V, and 2.0 V respectively with a high energy density of 7.4 Wh/kg with 1 M Na_2SO_4, but shown good capacitive retention for 6 M KOH [27]. Corn cob wastes obtained at 1000 °C from a gasifier showed higher micropore volume and high specific capacitance of 130 F g^{-1} (20 mV s^{-1}) when tested using the 3 and 2 electrodes electrochemical workstation [28].

This study aims at utilizing the alkali catalyzed hydrothermal biochar as an adsorbent for heavy metals such as Copper and Zinc and the suitability of used adsorbents as active material in supercapacitors.

2. MATERIALS & METHODS

2.1. Materials

Prosopis juliflora wood cutting obtained from Thoppupalayam, Perundurai, Tamil Nadu, India (Coordinates: 11°16'47.0"N 77°36'41.8"E) was cleaned using a blade to remove the exterior branches and spikes. The dried wood cutting was further broken into smaller pieces and was grounded in a hammer mill. The resulting product with particles of size 1 mm to 0.6 mm that passes through British Standard Mesh #16 and retained in #25 was separated in a sieve shaker and packed as 20 grams each in an air-tight polyethylene pouch. Other chemicals required are NaOH, KOH (Merck); HCl, H_2SO_4 (Surya Fine Chem, Pune), $ZnCl_2$, $CuCl_2.2H_2O$ (Labo Chemie Pvt. Ltd., Mumbai), and Rubber solution No.4 (Paramount Industries, Chennai). All chemicals used are of analytical grade.

2.2. Experimental Procedure

2.2.1. HTC of Biomass

A typical HTC process of wet biomass is done at an elevated temperature of 180 to 260 ℃, high pressure of 2–15 MPa, and reaction time from 5 min to several hours [29]. Although the reaction temperature and time are influencing parameters, the temperature is the most prominent and important parameter that alters the characteristics of the HTC products [30]. The biomass to water loading in a typical HTC process ranges from 3 to 10 times the dry mass of biomass [31][32]. HTC was performed with 20 g biomass and a specified amount of water (4 to 8 water loading in biomass mL g^{-1}) at different temperatures from 200 to 300 ℃ in a 600 mL closed hydrothermal bomb. The experiments were also performed with 5 wt% loading of KOH alkali catalyst and the resulting biochar is represented as PJ250-KOH HTC denoting that the hydrothermal biochar from *Prosopis juliflora* was obtained at 250 ℃ in the presence of KOH as the catalyst.

Kambo. H and Dutta. A [33] identified some of the important parameters, especially for hydrothermal carbonization like mass yield, and carbonation ratio was calculated using the following Equations. (1) and (2).

$$Mass\ Yield\ (\%) = \frac{Mass\ of\ dried\ biochar}{Mass\ of\ dried\ raw\ feedstock} \times 100 \quad (1)$$

$$Carbonization\ Ratio = \frac{\%Carbon\ in\ the\ biochar}{\%Carbon\ in\ the\ feed} \times \frac{Mass\ of\ dried\ biochar}{Mass\ of\ dried\ raw\ feedstock} \quad (2)$$

2.2.2. Effect of process parameters and process optimization using response surface methodology

Although the parameters temperature, reaction time, and water loading in biomass can be studied separately, the Response surface methodology helps us to understand both the individual and the interactive nature of these parameters over mass yield and carbonization ratio. Table 1 shows the 17

experimental runs with 5 central points computed by three-factor Box-Behnken Design (BBD) using Design Expert 8.0.7.1 software (Stat-Ease, Minneapolis, USA) by fixing the -1 and +1 levels of the independent variables i.e Factor 1 – Temperature: 200°C and 300°C, Factor 2 – Reaction time: 15 min and 45 min and, Factor 3 – Water Loading: 4 and 8 mL per g of biomass. In this design, the middle i.e. 0 level is the arithmetic mean of the extreme values.

A second-order polynomial equation used to calculate the response surface to all linear, square, and interaction terms is given as Equation. (3).

$$R = \alpha_0 + \sum_{l=1}^{k} \alpha_l x_{li} + \sum_{l=1}^{k} \alpha_{ll} x_{li}^2 + \sum_{l=1}^{k-1} \sum_{m=l+1}^{k} \alpha_{lm} x_{li}\, x_{mi} + \varepsilon_i \quad (3)$$

where R is the response for mass yield (MY) and carbonization ratio (CR); α_0 is the intercept coefficient; α_l, α_{ll}, and α_{lm} are interaction coefficients for linear, quadratic, and second-order terms of the developed model respectively; x_{li}, and x_{mi} are process variables (l and m range from 1 to k); k is the number of independent parameters and ε_i is the error [34].

The final model equation for three independent process parameters (k) i.e. temperature, reaction time, and water loading in biomass with the error term is given by Equation. (4).

$$R = \alpha_0 + \alpha_1 x_1 + \alpha_2 x_2 + \alpha_3 x_3 + \alpha_{11} x_1^2 + \alpha_{22} x_2^2 + \alpha_{33} x_3^2 + \alpha_{12} x_1 x_2 + \alpha_{13} x_1 x_3 + \alpha_{23} x_2 x_3 + \varepsilon_i \quad (4)$$

The adequacy of the model is also checked with Analysis of Variance (ANOVA) and the interaction of each parameter is also found from the F-values and the significance of terms is found from the p-value which must be below 0.05.

2.2.3. Adsorption studies and characterization of used adsorbent

Adsorption studies were carried out using a 60 mg L^{-1} aqueous solution of Copper and Zinc chloride prepared from the standard stock solution. 0.1 g of adsorbent was used to treat 250 mL of the solution and the equilibrium adsorption studies were carried out at different adsorption times i.e. 15, 30, 60, 90, 120, 150, 240, and 1440 min; an initial concentration of 15, 30, 60, 100, 200 and 300 mg L^{-1}. The solution was then filtered using 0.4 μm Whatman filter paper and was tested using Atomic Absorption flame Spectrophotometry (AAS) to measure the adsorption capacity of biochar and its removal percentage of Copper and Zinc respectively. The adsorption studies were performed at a pH of 6.0 for Copper and a pH of 7.0 for Zinc because the adsorbent surface becomes more positive charged at lower pH and on the increase of pH to 6.0 – 7.0 it made the adsorbent surface negatively charged aiding more removal of M(II) ions [35][36][37]. The pH adjustment of the initial aqueous solution was done using 0.1 M HCl and 0.1 M NaOH. Once the hollow cathode lamp was lit the system was allowed for 30 min warm-up and the blank solution was aspirated to set the zero. A five-point calibration using 20, 10, 5, 2.5, and 1.25 mg L^{-1} standard solutions was made and the system was calibrated before aspirating the unknown samples. The amount of Copper or Zinc adsorbed by the *Prosopis juliflora* HTC biochar (PJ250-CuAD and PJ250-ZnAD) and metal removal percentage was calculated using the Equations. (5) and (6).

$$Adsorption\ Capacity, Qe\ (mg\ L^{-1}) = \frac{(C_o - C_e)}{m} \times V \quad (5)$$

$$Metal\ Removal\ Percentage\ (\%)\ = \frac{(C_o - C_e)}{C_o} \times 100 \quad (6)$$

Where, m (g) is the dosage of biochar adsorbent, V (L) is the volume of solution, C_O (mg L^{-1}) is the initial metal concentration of the solution and C_e (mg L^{-1}) is the metal concentration of the solution at the state of equilibrium.

The data obtained at 25℃ were fitted to isotherm models, i.e. Langmuir and Freundlich, which are explained in Equations. (7)-(9). The pseudo-first-order kinetic model, pseudo-second-order kinetic model, and factorial power model were used to study the adsorption kinetics of Cu(II) and Zn(II), which are given as Equations. (10), (11), and (12) respectively.

$$\frac{C_e}{q_e} = \frac{1}{b\ q_{max}} + \frac{C_e}{q_{max}} \quad (7)$$

$$K_L = \frac{1}{1 + (b\ C_o)} \quad (8)$$

$$q_e = k_F C_e^{1/n} \quad (9)$$

$$\log(q_e - q_t) = \log\ q_e - \frac{k_{ad} t}{2.303} \quad (10)$$

$$\frac{t}{q_t} = \frac{1}{k_2 {q_e}^2} + \frac{t}{q_e} \quad (11)$$

$$\ln qt = \ln K + \Upsilon \ln t \quad (12)$$

where q_e is the adsorption capacity (mg g^{-1}) at equilibrium which is the amount of metal ion adsorbed (mg g^{-1}) at any instant of time, C_e is the concentration of the solution at equilibrium, q_{max} represents the maximum adsorption capacity and b is the Langmuir constant, C_0 is the initial concentration of the Cu(II) and Zn(II) aqueous solution. The value K_L indicates the type of isotherm and for it to be reversible (K_L=0), favorable (0< K_L<1), linear (K_L=1), or unfavorable (K_L>1); k_F and n are Freundlich constants; k_{ad} (L min^{-1}) is the rate constant of the pseudo-first-order adsorption process, k_2 (L min^{-1}) is the rate constant of the pseudo-second-order adsorption process, ϒ and K are constants of factorial power model.

0.5 g of used adsorbent i.e. the preadsorbed biochar was taken in 100 ml of 0.1 N H_2SO_4 for copper and 0.1 N HCl for zinc with the pH of 2 and shaken at 120 rpm for 6 h. The desorbed adsorbent was washed repeatedly 5 times with distilled water to remove any residual desorbing solution and dried is placed into an aqueous metal solution for the next adsorption cycle [38][39].

2.2.4. Fabrication of Supercapacitor electrodes

The used adsorbent collected as a residue during filtration was dried at 150°C in a hot air oven; ground and stored. The *Prosopis juliflora* HTC biochar (without catalyst), KOH catalyzed HTC biochar, Copper adsorbed KOH HTC biochar (CuAD5) and Zinc adsorbed KOH HTC biochar (ZnAD5) powders as an active material for the supercapacitor electrode. The working electrode was assembled along with Ag / AgCl as reference electrode and Platinum (Pt) wire as counter electrode in a 3 electrode system

with 6 M KOH as the electrolyte to perform the electrochemical analysis [40]. The working electrode was prepared by mixing the active material (about 250 μg) with the Rubber solution No.4 in a weight ratio of 40:60. The semi-solid mixture was coated using a brush on a graphite lead electrode, which acts as the current collector and it was dried at room temperature for 30 min [41]. The electrochemical properties of this composite were tested for Cyclic Voltammetry (CV), Galvanostatic Charge-Discharge (GCD), and Electrochemical Impedance Spectroscopy (EIS) in a potential range of -1.5 to 2 V using an electrochemical workstation (OrigaFlex - OGF500, France, potentiostat-galvanostat). Some of the important electrochemical terms and formulas representing the electrochemical properties are given below in Equations. (13) to (16).

$$Charge\ (A) = \frac{Intergral\ Area\ of\ the\ CV\ curve}{2\ \times Scan\ Rate} \tag{13}$$

$$Capacitance = \frac{Charge}{Potential\ window} \tag{14}$$

$$Specific\ capacitance\ (F\ g^{-1}) = \frac{Capacitance}{Mass\ of\ active\ material} \tag{15}$$

$$Specific\ capacitance\ (F\ g^{-1}) = \frac{Charge(or)Discharge\ current\ \times Discharge\ time}{Mass\ of\ electrode\ \times Potential\ window} \tag{16}$$

3. RESULTS & DISCUSSION

3.1. HTC-BBD Model fitting

Table 1. HTC-BBD Experimental Runs and Model Responses

Run Number	Factor 1- A: Temperature (°C)	Factor 2-B: Reaction Time (min)	Factor 3-C: Water Loading (mL g^{-1})	Actual Mass Yield (%)	Actual Mass Yield (%)	Actual Carbonization Ratio	Predicted Carbonization Ratio
1	200	45	6	57.4	58.34	1.1	1.1
2*	250	30	6	54.45	54.13	1.19	1.2
3	300	15	6	43.1	42.16	1.21	1.21
4	250	45	8	51	50.3	1.2	1.2
5*	250	30	6	53.85	54.13	1.2	1.2
6	250	15	4	51.1	51.8	1.15	1.15
7	300	45	6	36.17	36.44	1.26	1.26
8*	250	30	6	53.69	54.13	1.2	1.2
9	200	30	4	57.1	56.67	1.08	1.08
10	200	30	8	57.2	56.96	1.07	1.08
11	300	30	4	36.84	37.08	1.26	1.25
12	250	45	4	49.8	49.29	1.16	1.16
13	200	15	6	58.1	57.83	1.05	1.05
14*	250	30	6	54.05	54.13	1.2	1.2
15*	250	30	6	54.62	54.13	1.19	1.2
16	300	30	8	38.56	38.99	1.24	1.24
17	250	15	8	52.5	53.01	1.11	1.11

* Central Points

The process parameters such as temperature (℃), reaction time (min), and water loading in biomass (mL g^{-1}) were analyzed, where the experimental mass yield (response 1) and carbonization ratio (response 2) were determined for the set of process 17 runs in total including 5 central points derived from the Box Behnken Design of experiments and were fed as inputs to obtain the mathematical model whose predicted values are given in Table 1.

The model adequacy was confirmed by fitting the experimental responses i.e mass yield and carbonization ratio with four polynomial models namely: linear, 2-factor interactive (2FI), quadratic and cubic models using the sequential sum of squares method and statistics tests where the results are given in the Model Summary Table 2. The model fitting study suggested that the quadratic model for both mass yield and carbonization ratio was highly suited for the hydrothermal carbonization study with a probability p-value less than 0.0001 and had maximum F-values of 61.24 and 36.39, while the cubic model was said to be aliased. P<0.0001 suggests that the model is statistically highly significant with the chance of being wrong being less than one in ten thousand[42]. Although the cubic model is aliased, solving such higher-order equations involves a further more complex process called quadrangulation and it resulted in many contortions [43].

Table 2. Sequential Model Summary for HTC Response Models

Source	Sum of Squares	df	Mean Square	F Value	p-value Prob > F
HTC Model 1 – Mass Yield					
Mean vs Total	43458.34	1	43458.34		
Linear vs Mean	721.60	3	240.53	23.493	< 0.0001
2FI vs Linear	10.37	3	3.4564	0.281	0.8375
Quadratic vs 2FI	118.26	3	39.4084	61.245	< 0.0001
Cubic vs Quadratic	3.88	3	1.2944	8.339	0.0339
Residual	0.62	4	0.1552		
Total	44313.05	17	2606.64		
HTC Model 2 – Carbonization Ratio					
Mean vs Total	23.2245	1	23.22		
Linear vs Mean	0.06123	3	0.02040	36.089	< 0.0001
2FI vs Linear	0.00162	3	0.00054	0.946	0.4548
Quadratic vs 2FI	0.00538	3	0.00179	36.3964	< 0.0001
Cubic vs Quadratic	0.00022	3	7.5E-05	2.5	0.1985
Residual	0.00012	4	3E-05		
Total	23.2931	17	1.37018		

The second-order polynomial equations for HTC Models i.e. mass yield (MY) and carbonization ratio (CR) in terms of coded values X_1-Temperature, X_2 - Reaction Time, and X_3-Water loading are given in the Equations. (17) and (18).

$$MY = 54.132 - 9.39125X_1 - 1.30375X_2 + 0.5525X_3 - 1.5575X_1X_2 + 0.405X_1X_3 - 0.05X_2X_3 - 4.55725X_1^2 - 0.88225X_2^2 - \quad (17)$$

$2.14975X_3^2$

$$CR = 1.196 + 0.08375X_1 + 0.025X_2 - 0.00375X_3 - 0.0025X_1X_3 + 0.02X_2X_3 - 0.01675X_1^2 - 0.02425X_2^2 - 0.01675X_3^2 \quad (18)$$

Table 3. ANOVA for Response Surface Quadratic Models MY and CR

Response 1 Mass Yield (MR)						
Source	Sum of Squares	df	Mean Square	F Value	p-value Prob > F	
Model	850.1995	9	94.46661546	146.8125	< 0.0001	significant
X_1-Temperature	705.5646	1	705.5646125	1096.532	< 0.0001	
X_2-Reaction Time	13.59811	1	13.5981125	21.13311	0.0025	
X_3-Water Loading in Biomass	2.44205	1	2.44205	3.79524	0.0924	
X_1X_2	9.703225	1	9.703225	15.07998	0.0060	
X_1X_3	0.6561	1	0.6561	1.019659	0.3462	
X_2X_3	0.01	1	0.01	0.015541	0.9043	
X_1^2	87.44643	1	87.44643184	135.9023	< 0.0001	
X_2^2	3.277327	1	3.277326579	5.093361	0.0586	
X_3^2	19.45863	1	19.45863184	30.24106	0.0009	
Residual	4.504155	7	0.643450714			
Lack of Fit	3.883275	3	1.294425	8.339293	0.0339	significant
Pure Error	0.62088	4	0.15522			
Cor Total	854.7037	16				
Response 2 Carbonization Ratio (CR)						
Source	Sum of Squares	df	Mean Square	F Value	p-value Prob > F	
Model	0.068231	9	0.007581275	153.823	< 0.0001	significant
X_1-Temperature	0.056113	1	0.0561125	1138.514	< 0.0001	
X_2-Reaction Time	0.005	1	0.005	101.4493	< 0.0001	
X_3-Water Loading in Biomass	0.000113	1	0.0001125	2.282609	0.1746	
X_1X_2	0	1	0	0	1.0000	
X_1X_3	2.5E-05	1	2.5E-05	0.507246	0.4994	
X_2X_3	0.0016	1	0.0016	32.46377	0.0007	
X_1^2	0.001181	1	0.001181316	23.96873	0.0018	
X_2^2	0.002476	1	0.002476053	50.23875	0.0002	
X_3^2	0.001181	1	0.001181316	23.96873	0.0018	
Residual	0.000345	7	4.92857E-05			
Lack of Fit	0.000225	3	7.5E-05	2.5	0.1985	not significant
Pure Error	0.00012	4	0.00003			
Cor Total	0.068576	16				

The model equations (19) and (20) providing the relationship between the process parameters (temperature-X_1, reaction time-X_2, and water loading in biomass-X_3) and the responses MY and CR were said to be adequate with F-values 146.81 and 153.82 respectively from the results obtained from

the ANOVA as given in Table 3. The second order-quadratic models for mass yield and carbonization ratio were found to have "Adjusted R-Squared" values (98.79, 98.85)% and "Predicted R-Squared" (92.61, 94.47)% with less than 10% deviation suggesting a better model equation can be developed for the given dataset with minimum error [44]. A minimum F-value was obtained during the lack of fit test for the quadratic models MY and CR indicating that they were having insignificant lack of fit of 8.34 and 2.5. This denotes that the models were studied relative to the pure error and the p-value from this test also suggested that there was a 3.39 and 19.85 % chance of insignificance for MY and CR respectively. These values are large which might be due to noise and thus the models were found to be fit [45]. The coefficient of determination (R^2) for MY and CR were 99.47 and 99.5%, which ensured that there is a satisfactory adjustment of the obtained quadratic models and thus the experimental data was said to have a high correlation with the predicted values as given in Table 1.

3.2. Effect of process parameters on hydrothermal carbonization

Both the individual and interaction of the process parameters were studied. Figures 1 (a), (b), and (c) provides the single factor influence on mass yield, and Figures 1 (e), (f), and (g) provide the single factor influence on carbonization yield for X_1, X_2, and X_3 respectively with other two kept constant.

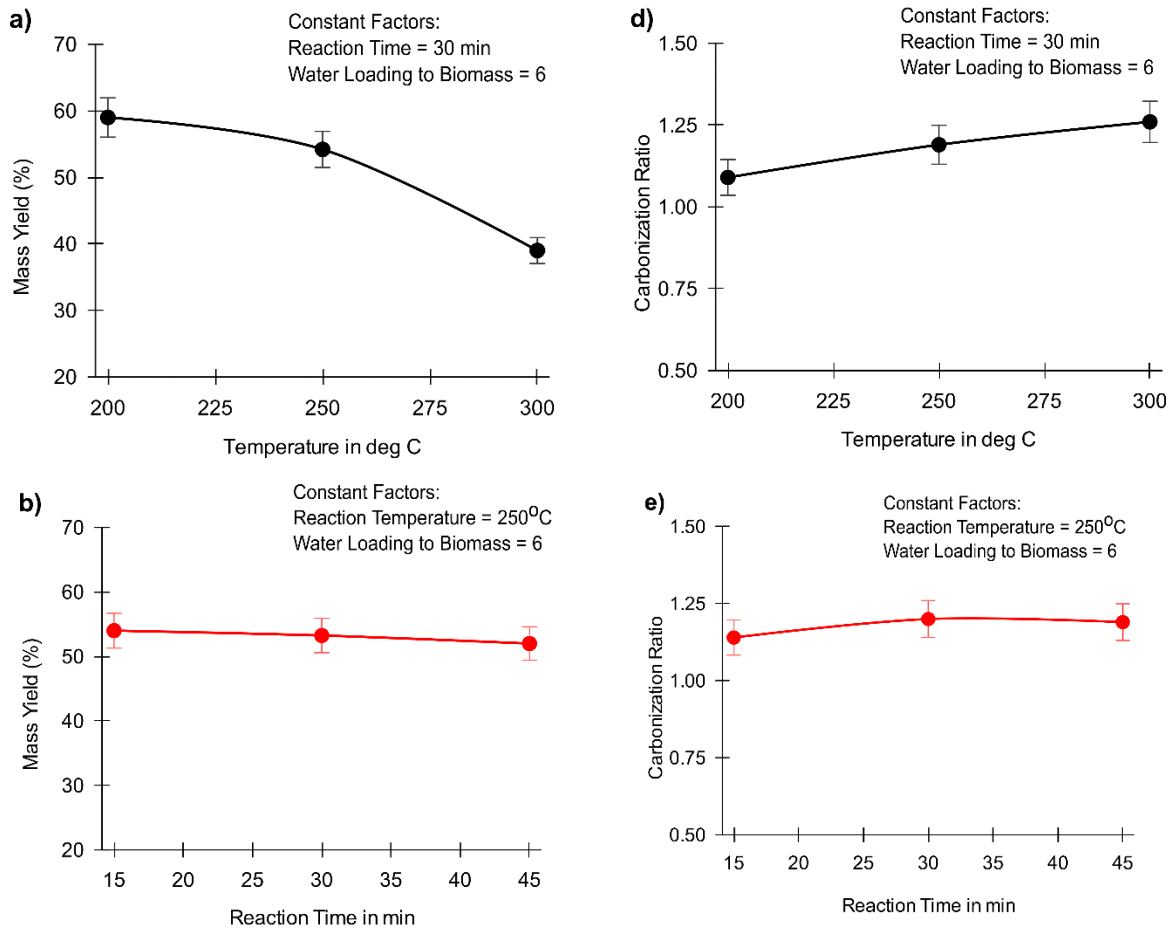

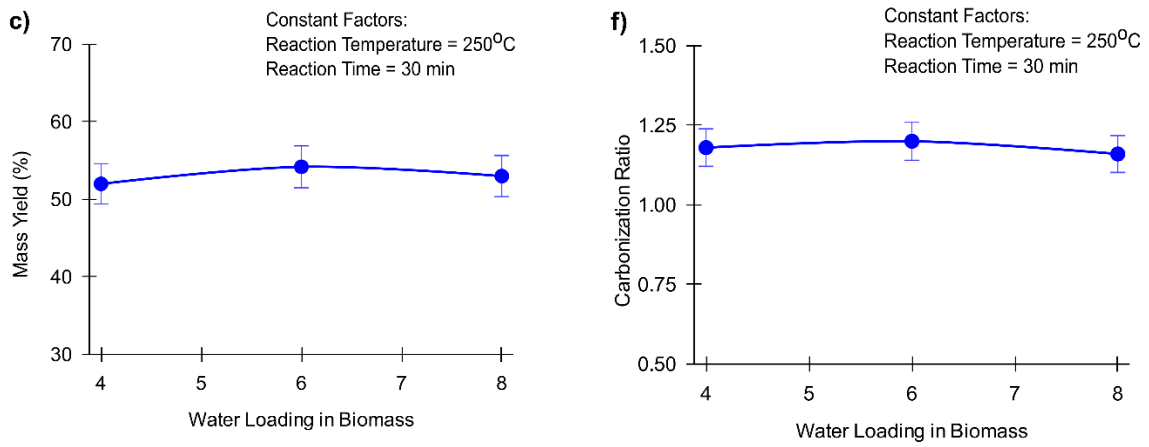

Figure 1 a), b), c) One-factor analysis of HTC on mass yield d), e), f) One-factor analysis of HTC on carbonization ratio

From the Figures 1 (a) and (d) it can be observed that the mass yield of the biochar decreases while the carbonization ratio increases in the biochar when the temperature is increased from 200 to 300℃ at a constant reaction time of 30 min and water loading in biomass at 6 mL g^{-1}. Similar observations were made for hydrothermal carbonization of waste wood i.e. on an increase of temperature from 180 to 260 ℃ the mass yield of the biochar decreased from 81.2 to 38.7%[46]. The same trend is observed in Figures 1 (b) and (e) when the reaction time is increased from 15 to 45 min at a constant temperature of 250℃ and water loading in biomass 6 mL g^{-1}. The increase in the reaction time resulted in decreases in the mass yield, an increase in carbon content, and an increase in the porosity[11][47]. From Figures 1 (c) and (f) it can be observed that the mass yield and carbonization ratio are almost the same and are not affected by the change in water loading in biomass from 4 to 8 mL g^{-1} at a constant temperature of 250℃ and reaction time 30 min. Furthermore, an increase in water loading might cause the shift of the process from carbonization to liquefaction[48]. From the ANOVA results the significant terms for the mass yield HTC model were X_1, X_2, X_{12}, X_1^2, and X_3^2 while for the carbonization ratio HTC model the significant terms were X_1, X_2, X_{23}, X_1^2, X_2^2, and X_3^2 with p-value less than 0.05. It is evident that from Figures 2 (a) and (d) when the temperature and reaction time was increased from 200 to 300℃ and 15 to 45 min respectively by keeping water loading in biomass as 6 mL g^{-1}, a negative effect i.e decrease in mass yield is observed while in contrary maximum carbonization ratio of 1.26 is obtained for the same condition suggesting the positive effect and both the factors are significant individually and are more interactive as reported by Mohammed et.al [49].

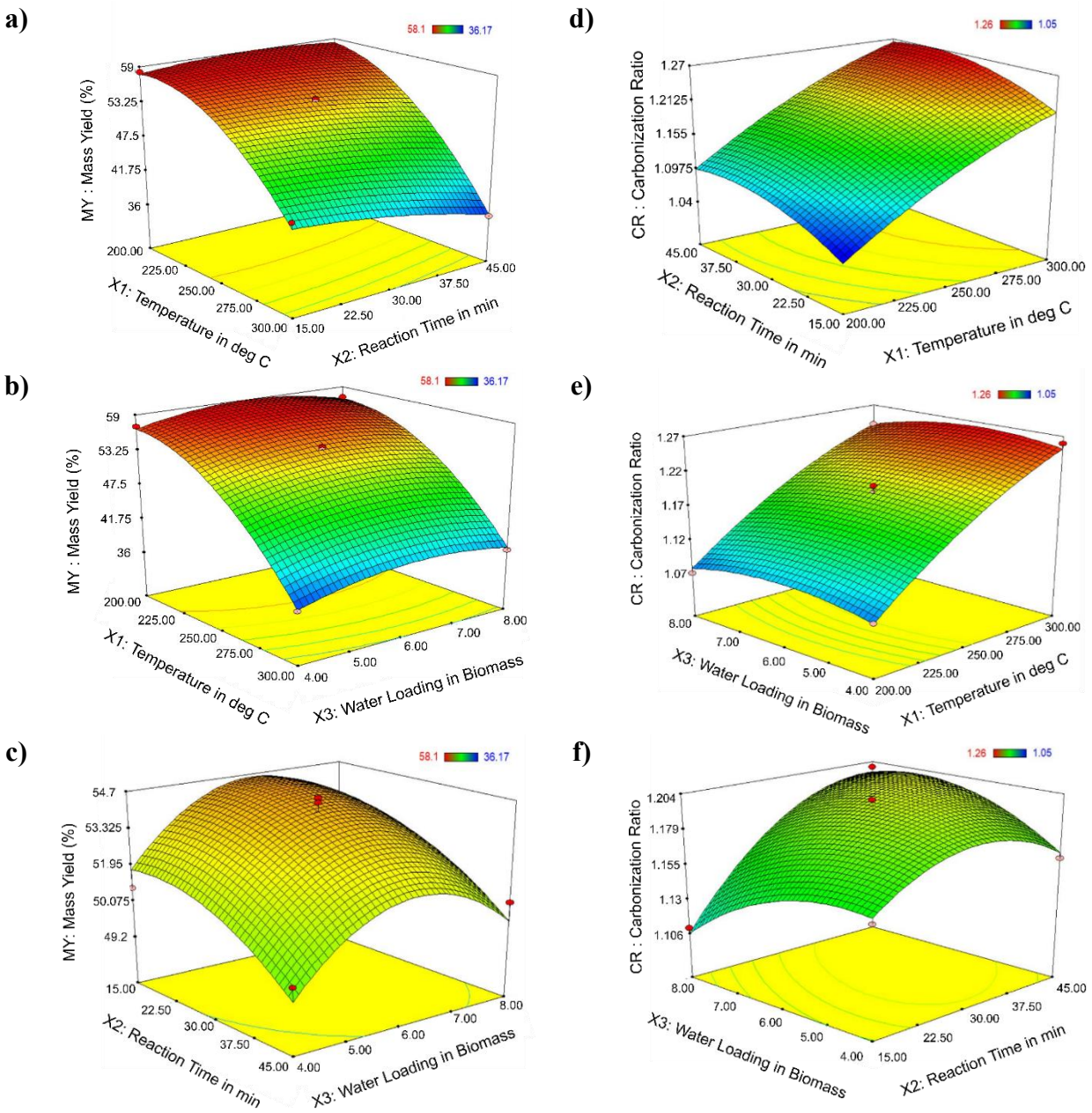

Figure 2 a),b),c) 3D Response Surface Plot for Mass Yield; d),e),f) 3D Response Surface Plot for Carbonization Ratio

The 3D response plots in Figs. 2 (b) and (e) demonstrate the mass yield decreased and carbonization ratio increased when the temperature and water loading in biomass was increased from 200 to 300℃ and 4 to 8 respectively by keeping reaction time as 30 min, where maximum mass yield was 58.1 % and the more significant factor is temperature and there is less interaction between temperature and water loading in biomass in the given range of study. The 3D response plots in Figures 2 (c) and (f) show that the when the reaction time and water loading in biomass were varied from 15 to 45 min and 4 to 8 mL g^{-1} at constant temperature i.e. 250℃ affects both mass yield and carbonization ratio in such a way that reaction time has a positive effect on carbonization ratio and negative effect on mass yield with good interaction with p-value less than 0.05 as confirmed from the ANOVA results[50][51].

3.3. Optimization of process parameters

The optimization study for the HTC of *Prosopis juliflora* was carried out to obtain the maximum mass yield and maximum carbonization ratio within the given range of process parameters. The process optimization of parameters: temperature (X_1), reaction time (X_2), and water loading in biomass (X_3) was done by solving the response Equations (19) and (20) for the given process conditions. The desirability was tested to find the optimum process condition to obtain both the objectives i.e. maximum mass yield and maximum carbonization ratio, which is more significant when there is more than one objective [22]. The process parameters X_1, X_2, and X_3 were kept in range with fixed importance of "+++", while the objectives were kept to maximize mass yield (lower limit: 36.17, higher limit: 58.1) and maximize carbonization ratio (lower limit: 1.05, higher limit: 1.26) with importance "+++++". The optimization resulted in 75.9 % desirability at a temperature of 250.09°C, a reaction time of 33.65 min, and water loading in biomass of 6.17 %w/v with a maximum mass yield of 53.77 % and maximum carbonization ratio of 1.20 as shown in Figure 3. Rather than showing the individual significance of temperature, reaction time and water loading in biomass towards the implementation of desirability function to the response surface methodology helped in getting a significant result on optimization with a good yield of biochar (53.77%) and with better carbonization ratio (1.2)[52]. The HTC was performed in triplets for the optimum conditions and the mass yield and carbonization ratio were confirmed as 53.5 ± 1.4 % and 1.2 ± 0.04.

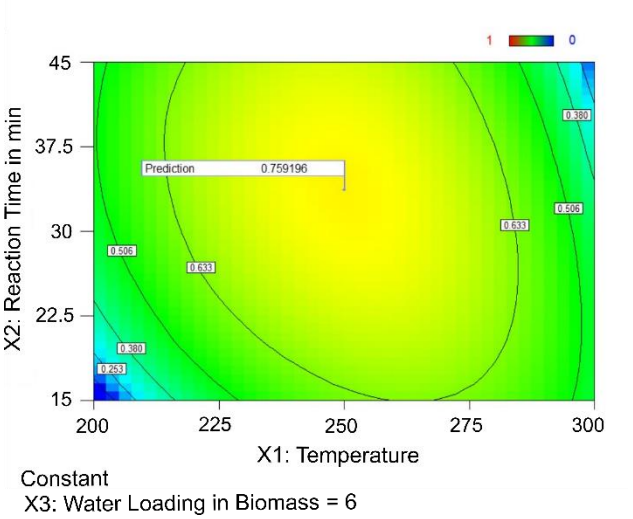

Figure 3. Desirability contour plot

3.4. Copper and Zinc Adsorption Studies

The alkali catalyzed HTC biochar was characterized by morphological characteristics, elemental metal composition, BET surface area, and its suitability for acting as an adsorbent were studied.

Adsorption studies were carried out using 250 mL aqueous solution of 60 ppm Copper and Zinc chloride with 0.1 g of adsorbent for different adsorption times i.e. 15, 30, 60, 90, 120, 150, 240, and 1440 min. The residual concentration of Cu(II) and Zn(II) in 60 ppm initial concentration aqueous

solution and respective removal percentage for various times (15, 30, 60, 90, 120, 150, 240, and 1440 min) using PJ250-KOH HTC biochar is illustrated in Figure 5 and it shows that within 120 min about 68.33% of Cu(II) and 60% Zn(II) is removed. The equilibrium concentration of the Cu(II) and Zn(II) adsorption were measured at 1440 min which is 12 and 18 ppm respectively. Adsorption studies were also carried out for different initial concentrations (15, 30, 60, 100, 200, and 300 ppm), and the respective adsorption capacity for 0.1 g adsorbent in 250 mL aqueous solution is determined and plotted in Figure 4. The adsorption capacity of Cu(II) and Zn(II) onto PJ250-KOH HTC biochar is given in Figure 5.

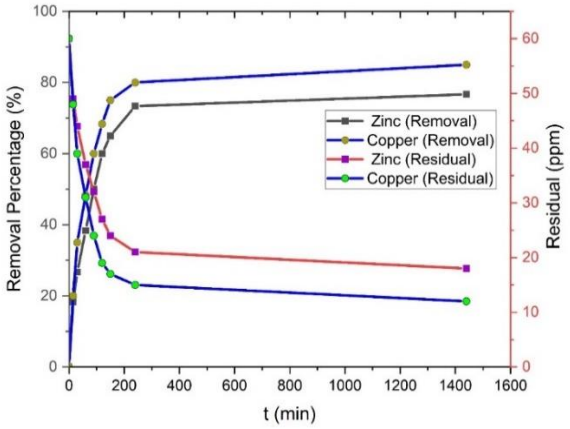

Figure 4 Residual concentration of Cu(II) and Zn(II) in solution and respective removal percentage for various times using PJ250-KOH HTC biochar

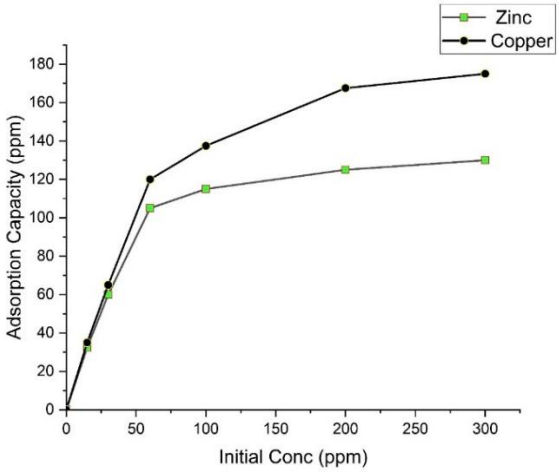

Figure 5 Cu(II) and Zn(II) adsorption capacity onto PJ250-KOH HTC biochar for various initial metal concentrations.

The equilibrium data were analyzed for PJ250-KOH HTC biochar as adsorbents for both Cu(II) and Zn(II) aqueous solutions and investigated using Freundlich and Langmuir isotherms and the constants are given in Table 4.

It was observed that the adsorption process was a very good fit for Langmuir isotherm and the maximum adsorption capacity of PJ250-KOH HTC biochar was found to be 217.39 mg g^{-1} and 149.25 mg g^{-1} for Cu(II) and Zn(II) aqueous solutions respectively. This value is less when compared to hydrochar produced from miscanthus obtained at 180°C with q_{max} as 301 mg g^{-1} for copper adsorption but more than that of hydrochar produced from *Nannochloropsis* sp. at 250°C with q_{max} as 12.56 mg g^{-1}

[53][54]. While another study shows that modified hydrochar with polyethyleneimine resulted in an adsorption capacity of 56.1 mg g^{-1} of Cu(II) and 207.6 mg g^{-1} of Zn(II) respectively [55]. The adsorption kinetics such as pseudo-first-order, pseudo-second-order, and factorial power model was also studied and the constants are given in Table 5 which shows that both copper and zinc adsorption follows pseudo-second-order kinetics.

Table 4. Isotherm constants for absorption of Cu(II) and Zn(II) onto HTC PJ250-KOH biochar

Isotherm Parameters	Langmuir			Freundlich		
	q_{max} (mg g^{-1})	K_L	R^2	k_F (L g^{-1})	n	R^2
Cu(II)	217.39	0.015	0.9904	10.373	1.89	0.9066
Zn(II)	149.25	0.025	0.9911	12.514	2.24	0.8482

Table 5. Kinetic constants for absorption of Cu(II) and Zn(II) onto HTC PJ250-KOH biochar

Kinetic Models/ Parameters	Pseudo First Order			Pseudo Second Order			Factorial Power		
	q_e (mg g^{-1})	k_{ad} (min^{-1})	R^2	q_e (mg g^{-1})	k_2 (min^{-1})	R^2	K (mg g^{-1})	ϒ	R^2
Cu(II)	38203.22	0.02764	0.9557	121.95	3439.92	0.9991	19.95	0.3048	0.8005
Zn(II)	33790.92	0.02556	0.9874	107.53	3850.16	0.9987	15.82	0.2957	0.7350

The desorption studies were performed for both PJ250-CuAD and PJ250-ZnAD and it was found that for every subsequent cycle of reused biochar efficiency decreased [56]. It was found that for PJ250-CuAD the Cu removal percentage reduced from 80% to 70.2% and for PJ250-CuAD the Cu removal percentage reduced from 73.33% to 59.5% after 5 cycles of recycling and reuse. Thus there is about a 12-19% reduction in the efficiency and these adsorbents (PJ250-CuAD5 and PJ250-ZnAD5) are hence not advised to be further used for the adsorption process. It is evident that the reusing of adsorbent reduces its efficacy during reuse but can produce a substance that might apply to some other application i.e. mercury adsorbed super adsorbent used as a catalyst for the transformation of phenylacetylene to acetophenone with a yield of 52% and Cadmium adsorbed fly ash composite material used as photocatalyst for methylene blue dye degradation [57][58].

a) b)

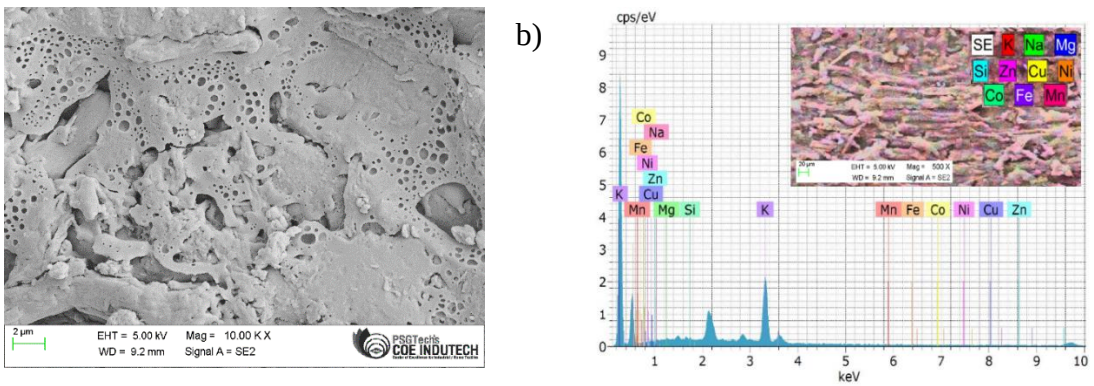

Figure 6 HTC-PJ250-KOH Biochar a) SEM Analysis Image b) EDAX spectrum

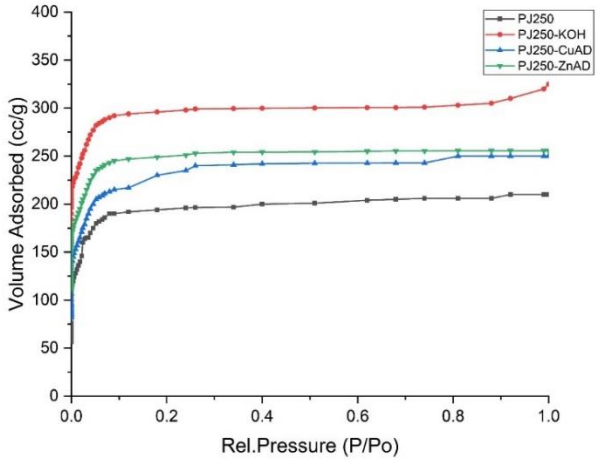

Figure 7 N_2 adsorption isotherms of *Prosopis juliflora* HTC Biochar PJ250 – HTC without KOH, PJ250 – HTC with KOH catalyst, PJ250 – Cu Adsorbed biochar, and PJ250 – Zn Adsorbed biochar

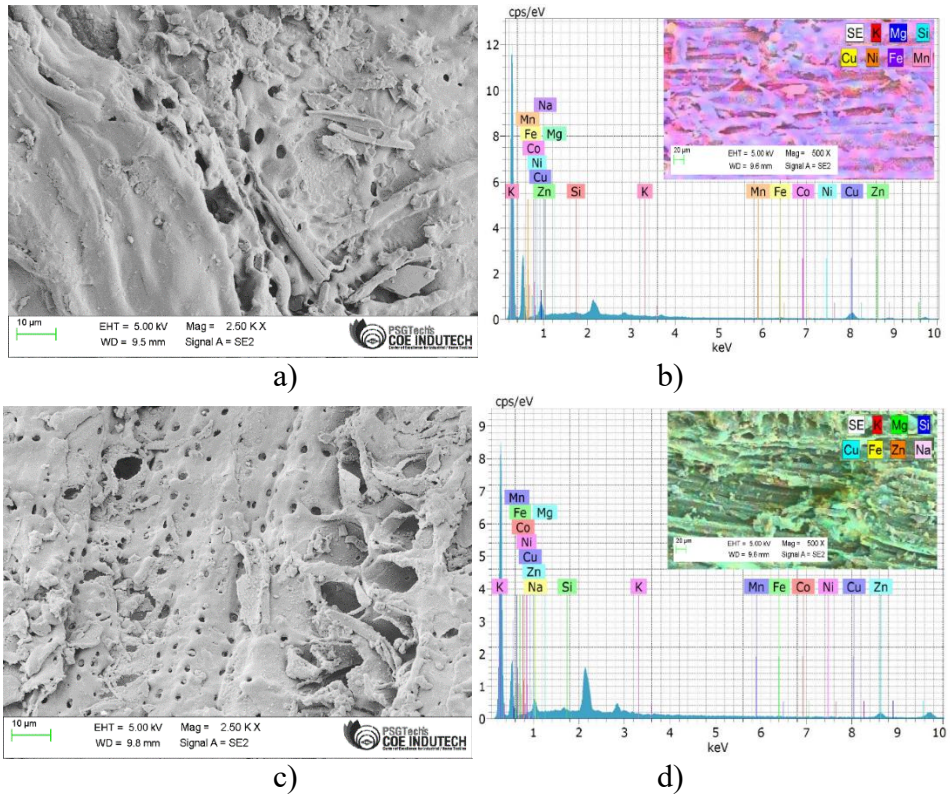

Figure 8 *Prosopis juliflora* KOH catalyzed HTC adsorbent produced at optimum conditions a) SEM analysis after Copper adsorption b) EDAX and mapping after Copper adsorption c) SEM analysis after Zinc adsorption d) EDAX and mapping after Zinc adsorption

The morphological surface of HTC char (PJ250), KOH catalyzed HTC char (PJ250-KOH), Cu adsorbed (PJ250-CuAD5) and Zn (PJ250-ZnAD5) adsorbed biochar derived from *Prosopis juliflora* is illustrated in the Figures 6 (a), 8 (a) and (c) respectively. The pores developed on the PJ250 are primarily

due to the disintegration of polysaccharides with the release of volatile matters [59]. The existence of heterogeneous, corrugated surface with low cavities are confirmed in the HTC processed biochar. However, considerable deviations are interpreted in KOH catalyst biochar (PJ250-KOH) which has flat layers, and corrugated ridges with a significant number of pores on its surface. Figure 7 shows the volume of nitrogen adsorbed for the given relative pressure (P/Po), where P is the partial saturation pressure of the adsorptive gas in equilibrium with the surface and Po is the gas saturation pressure and it is observed that there is a significant increase in the volume of nitrogen adsorbed due to the activation process, where new pores were developed on the surfaces. The pores and the cracks in activated biochar promote the adsorption characteristic of biochar and it is similar to that of the structure as obtained from alkali-activated (NaOH) HTC biochar from sugarcane bagasse [60].

After adsorption studies, most pores are plugged by Cu(II) and Zn(II) and it is observed that a high degree of Cu and Zn is absorbed on the surface of the biochar as graphically shown in Figure 6 (b), Figures 8 (b) and (d) respectively which is similar to the observation made on the Zn(II) on bamboo sawdust HTC biochar [61]. However other elements such as Mn, Mg, Ni, Fe, Si, K, Na, and Co were also quantified through EDAX and given in Table 6.

Table 6 Elemental Metal Composition of HTC KOH Biochar and Biochar after Cu(II) and Zn(II) adsorption

	Normalized Weight Percentage		
Elements	**PJ250-KOH**	**PJ250-CuAD5**	**PJ250-ZnAD5**
Manganese	0.95	0.6	0
Magnesium	2.54	14.73	12.89
Copper	1.05	69.37	0.56
Zinc	3	0	54.77
Nickel	0.29	0.93	0
Iron	0.98	2.99	1.6
Silicon	0.28	9.35	7.96
Potassium	88.03	2.03	0.39
Sodium	2.87	0	21.82
Cobalt	0	0	0

3.5. Testing fabricated carbon composite as Supercapacitor material

Cyclic voltammetry is considered to be a perfect tool to study and analyze the electrochemical performance of the samples with a potential window versus Ag/AgCl at a scan rate of 5 mV/s, in a three-electrode electrochemical workstation with Pt as a counter electrode using 6M KOH electrolyte [62].

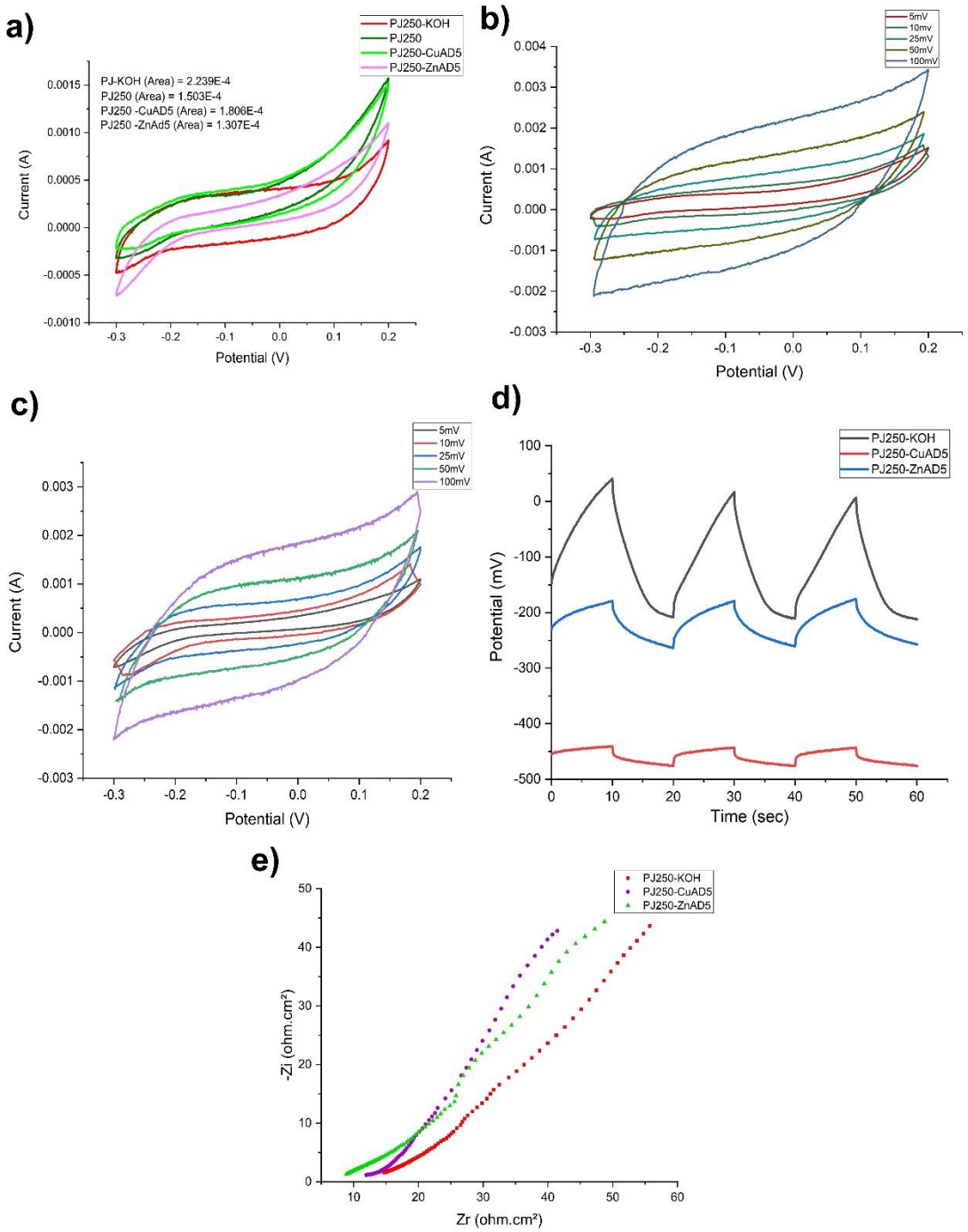

Figure 9 a) CV Curve for PJ250, PJ250-KOH, PJ250-CuAD5 and PJ250-ZnAD5 composites at 5 mV/s, b) CV Curve for PJ250-CuAD5 composite for scan rates 5, 10, 25, 50, 100 mV/s, b) CV Curve for PJ250-ZnAD5 composite for scan rates 5, 10, 25, 50, 100 mV/s, d) GCD curve for PJ250-KOH, PJ250-CuAD5 and PJ250-ZnAD5 composites, e) Nyquist plot for PJ250-KOH, PJ250-CuAD5 and PJ250-ZnAD5 composites

The normal HTC biochar, alkali HTC biochar, Copper adsorbed biochar and Zinc adsorbed biochar composites i.e. denoted as PJ250 (without catalyst), PJ250-KOH, PJ250-CuAD5, and PJ250-ZnAD5 were used as active electrode material for supercapacitor and the performance was studied through standard CV, GCD, and EIS.

Figure 9 (a) illustrates the CV curve of all the prepared electrode material with a potential range of -0.3 to +0.2 V (scan rate, 5 mV s^{-1}). The CV forms of the PJ250, PJ250-KOH, PJ250-CuAD5, and PJ250-ZnAD5 change tremendously and are quasi rectangular, representing EDL capacitive behavior with a specific capacitance of 120.24 F g^{-1}, 179.12 F g^{-1}, 144.48 F g^{-1}, and 104.56 F g^{-1} respectively calculated using the Eqns. (15) to (18). It is evident that from the N_2 adsorption plot Figure 4, it is noted that the absolute area obtained from PJ250-KOH is larger i.e. about 300 cc g^{-1} compared to other materials from the CV curve, at the same scan rate from its higher specific capacitance. Figure 9 b) and c) show the CV curve for Copper adsorbed HTC biochar and Zinc adsorbed HTC biochar composites respectively for various scan rates such as 5, 10, 25, 50, and 100 mV/s denoting various current densities in the potential window of -0.3 to +0.2 V.

Figure 9 (d) shows the GCD curve for PJ250-KOH, PJ250-CuAD5, and PJ250-ZnAD5 composites with constant or stable charging and discharging time of 10 s. The potential window for PJ250-KOH, PJ250-CuAD5, and PJ250-ZnAD5 composites was found to be 249.29 mA, 35.16 mA, and 84.47 mA respectively which decreased and stabilized from the second cycle onwards to 227.83 mA, 33.34 mA, and 81.73 mA respectively. The specific capacitance calculated for PJ250-KOH, PJ250-CuAD5, and PJ250-ZnAD5 composites from the GCD curve was 40.11 F g^{-1}, 284.41 F g^{-1}, and 118.38 F g^{-1} respectively. The EIS analysis was carried out in the frequency range of 0.1 to 100 kHz and the data were plotted using the Nyquist plot which has +Z real on the x-axis and –Z imaginary on the y-axis as shown in Figure 9 (e). The starting straight line in the plot which is almost parallel to the y-axis corresponds to the Warburg resistance and the frequency slope is witnessed to be around 45^o which supports the porous nature of the active materials [63] Although the initial resistance for PJ250-KOH was comparatively high, its porous nature made it suitable for charge storage. It was also observed that the initial resistance of PJ250-ZnAD5 was less compared to PJ250-CuAD5, yet the conductive nature of Cu(II) calcined along the pores of the adsorbent made it have more specific capacitance, and yet there is a drop in its potential window due to more fused pores during the adsorption process as seen from the Figure 8 (a).

Table 7. Adsorption and Electrochemical performance of adsorbents

Category/ Application	**Metal/ Oxide/ Ion/ Doped /Dye Adsorbent**	**Adsorption capacity/ Impregnation with conditions**	**Specific capacitance**	**Electrolyte**	**Ref**
Used and discarded Supercapacitor carbon to adsorbent	Ag(I)	104.0 mg/g (2 g for 1000 mL, 2000 mg L^{-1} initial concentration)	-	-	[64]
Used and discarded Supercapacitor carbon to adsorbent	Cr(VI)	96.3 mg g^{-1} (2 g for 1000 mL, 2000 mg L^{-1} initial concentration)	-	-	[64]

Metal Doped material for supercapacitor	Cu(II)	7% (80℃ for 12 h drying, and calcination at 200℃ for 5 h)	94 F g^{-1} at 0.7 A g^{-1}	1 M H_2SO_4	[65]
Metal Doped material for supercapacitor	Mn(II)	7% (80℃ for 12 h drying, and calcination at 200℃ for 5 h)	107 F g^{-1} at 0.7 A g^{-1}	1 M H_2SO_4	[65]
Metal Doped material for supercapacitor	Zn(II)	7% (80℃ for 12 h drying, and calcination at 200℃ for 5 h)	88 F g^{-1} at 0.7 A g^{-1}	1 M H_2SO_4	[65]
Dye adsorbed material as supercapacitor	MB onto Tissue paper derived AC	24.36 mg g^{-1} (60 mg L^{-1} initial concentration in 100 min)	260 F g^{-1} at 0.5 A g^{-1}	1 M H_2SO_4	[63]
Dye adsorbed material as supercapacitor	MB onto Hardboard paper derived AC	- (60 mg/L initial concentration in 100 min)	155 Fg^{-1} at 0.5 A/g^{-1}	1 M H_2SO_4	[63]
Adsorbent as supercapacitor material	Cr(VI)	142.1 mg g^{-1} (10 mg in 20 mL metal ions solution for 11 h in 200 rpm)	144.9 F g^{-1} at 2 mV s^{-1}	1 M H_2SO_4	[66]
Adsorbent as supercapacitor material	Cu(II)	123.7 mg g^{-1} (10 mg in 20 mL metal ions solution for 11 h in 200 rpm)	114.9 F g^{-1} at 2 mV s^{-1}	1 M H_2SO_4	[66]
Used Adsorbent as supercapacitor	Cu(II)	217.39 mg g^{-1} (60 mg L^{-1} initial concentration in 250 mL solution for 1440 min)	144.48 F g^{-1} at 1 A g^{-1}	6 M KOH	This work
Used Adsorbent as supercapacitor	Zn(II)	149.25 mg g^{-1} (60 mg L^{-1} initial concentration in 250 mL solution for 1440 min)	104.56 F g^{-1} at 1 A g^{-1}	6 M KOH	This work

MB-Methylene Blue, AC-Activated Char

It can be observed from Table 7 that the PJ250-HTC biochar has good adsorption capacity and also good electrochemical properties even after the pores are saturated with Cu(II) and Zn(II) ions. This work suggests a new strategy for the utilization of waste adsorbent impregnated with heavy metal ions

for energy devices, thereby opening a new way to reduce the environmental pollutants and turn them into a source of clean energy.

4. CONCLUSION

i. *Prosopis juliflora* was identified as a good candidate for producing good quality biochar through the HTC process.

ii. The HTC optimization of *Prosopis juliflora* using response surface methodology resulted in 75.9 % desirability at temperature 250.09°C, reaction time 33.65 min, and water loading in biomass 6.17 mL g^{-1} with a maximum mass yield of 53.77 % and maximum carbonization ratio of 1.20.

iii. The adsorption studies for removal of Cu(II) and Zn(II) from aqueous solution using KPH catalyzed HTC biochar resulted in a very good fit for Langmuir isotherm with R^2 values 0.9904 and 0.9911 following pseudo-second-order kinetics with R^2 values 0.9991 and 0.9987 respectively.

iv. The maximum adsorption capacity of PJ250-KOH HTC biochar was found to be 217.39 mg g^{-1} and 149.25 mg g^{-1} for Cu(II) and Zn(II) aqueous solutions respectively.

v. The PK250, PJ250-KOH, PJ250-CuAD5, and PJ250-ZnAD5 HTC biochar composites showed EDL capacitive behavior producing quasi rectangular shape curves with a specific capacitance of 120.24 F g^{-1}, 179.12 F g^{-1}, 144.48 F g^{-1}, and 104.56 F g^{-1} respectively.

ACKNOWLEDGMENTS

The author would like to acknowledge the facility rendered by Kongu Engineering College for providing the infrastructure and utilizing the electrochemical workstation sanctioned by the Department of Science and Technology, Government of India under the FIST Scheme (2018). Also, we acknowledge the instrumental analysis facility rendered by the Centre of Excellence for Industrial Textiles promoted by Ministry of Textiles, Government of India established at PSG Institute of Technology and Applied Research, Coimbatore.

FUNDING

The authors declare that no funds, grants, or other support were received during the preparation of this manuscript.

COMPETING INTERESTS

The authors have no relevant financial or non-financial interests to disclose.

AUTHOR CONTRIBUTIONS

Mothil Sengottian and Chitra Devi Venkatachalam contributed to the study's conception and design. Material preparation, data collection, and analysis were performed by Mothil Sengottian, and graphical contents and illustrations were performed by Mothil Sengottian and Sathish Raam Ravichandran. The first draft of the manuscript was written by Mothil Sengottian and all authors reviewed and approved the final manuscript.

References

1. J. Castro-Gutiérrez, A. Celzard, V. Fierro, *Front. Mater.*, 7 (2020) 1–25.
2. E. Frackowiak, *Phys. Chem. Chem. Phys.*, 9 (2007) 1774–1785.
3. V. Chitra Devi, S. Mothil, R. Sathish Raam, K. Senthilkumar, R. Praveen Kumar, B. Bharathiraja, R. Kataki, V.S. Moholkar (Eds.), Biomass Valorization to Bioenergy, Springer Singapore, (2020) Singapore, pp. 45–63.
4. C.D. Venkatachalam, M. Sengottian, S.R. Ravichandran, M. Jerold, S. Arockiasamy, V. Sivasubramanian (Eds.), Bioprocess Eng. Bioremediation Valorization Manag. Tech., Springer International Publishing, (2020) Cham, pp. 201–224.
5. W. Xiang, X. Zhang, J. Chen, W. Zou, F. He, X. Hu, D.C.W. Tsang, Y.S. Ok, B. Gao, *Chemosphere*, 252 (2020) 126539.
6. Y. Jing, Y. Zhang, I. Han, P. Wang, Q. Mei, Y. Huang, *Sci. Rep.*, 10 (2020) 1–12.
7. A. Kumar, T. Bhattacharya, S.M. Mozammil Hasnain, A. Kumar Nayak, M.S. Hasnain, *Mater. Sci. Energy Technol.*, 3 (2020) 905–920.
8. G. Ischia, L. Fiori, *Waste and Biomass Valorization*, 12 (2021) 2797–2824.
9. K. Krysanova, A. Krylova, V. Zaichenko, *Fuel*, 256 (2019) 115929.
10. X. Jian, X. Zhuang, B. Li, X. Xu, Z. Wei, Y. Song, E. Jiang, *Environ. Technol. Innov.*, 10 (2018) 27–35.
11. M. Sengottian, C.D. Venkatachalam, S.R. Ravichandran, S. Sekar, A. Thirumoorthi, K.A. Selvakumar, L. Sankaralingam, *AIP Conf. Proc.*, 2240 (2020).
12. M. Bai, B. Wilske, F. Buegger, J. Esperschütz, C.I. Kammann, C. Eckhardt, M. Koestler, P. Kraft, M. Bach, H.-G. Frede, L. Breuer, *Plant Soil*, 372 (2013) 375–387.
13. D. Busch, A. Stark, C.I. Kammann, B. Glaser, *Ecotoxicol. Environ. Saf.*, 97 (2013) 59–66.
14. Y. Gao, Y. Liu, G. Zhu, J. Xu, H. xu, Q. Yuan, Y. Zhu, J. Sarma, Y. Wang, J. Wang, L. Ji, *Energy*, 165 (2018) 662–672.
15. M. Singh, R. Arunachalam, L. Kumar, *Ecol. Inform.*, 64 (2021) 101386.
16. S. Arandhara, S. Sathishkumar, S. Gupta, N. Baskaran, *Eur. J. Wildl. Res.*, 67 (2021) 48.
17. R. Murugan, F. Beggi, N. Prabakaran, S. Maqsood, R.G. Joergensen, *Soil Ecol. Lett.*, 2 (2020) 61–72.
18. J.A. de M. Carneiro-Junior, G.F. De Oliveira, C.T. Alves, E.A. Torres, *Energies*, 14 (2021) 1–18.
19. Z. Kiflie, M. Solomon, S.K. Kassahun, *Biomass Convers. Biorefinery* (2021).
20. A. Chandrasekaran, S. Subbiah, P. Bartocci, H. Yang, F. Fantozzi, *Fuel*, 285 (2021) 119095.
21. R. Chandran, R. Kaliaperumal, S. Balakrishnan, A.J. Britten, J. MacInnis, M. Mkandawire, *Energy*, 190 (2020) 116387.
22. C.D. Venkatachalam, M. Sengottian, S.R. Ravichandran, *Period. Polytech. Chem. Eng.*, 65 (2021) 105–115.
23. D.A. Iryani, S. Kumagai, M. Nonaka, K. Sasaki, *Waste and Biomass Valorization*, 8 (2017) 1941–1951.
24. K. Macdermid, W. Ranjan, P. Animesh, *Waste and Biomass Valorization*, 12 (2021) 2171–2186.
25. L. Qin, Y. Wu, Z. Hou, S. Zhang, E. Jiang, *J. Ind. Eng. Chem.*, 102 (2021) 195–205.
26. G.M. Kalu-Uka, S. Kumar, A.C. Kalu-Uka, S. Vikram, G.O. Ihekweme, N. Ranjan, E.N. Anosike-Francis, G. Prajapati, A. Nduba, A.P. Onwualu, S. Kumar, *Waste and Biomass Valorization*, 13 (2022) 2689–2704.
27. I. Izwan, M. Nurul, K. Mohd, Z. Rajan, *Waste and Biomass Valorization*, 10 (2020) 1731–1740.
28. D.C.M. Casillas, I. Mascorro, G. Maria, L.B. Mendiola, G. Palestino, E. Quiroga, G. Jojhar, E.P. Sussoni, A. Guillén, L. Jesús, *Waste and Biomass Valorization*, 12 (2021) 4123–4140.
29. A. Funke, F. Ziegler, *Biofuels, Bioprod. Biorefining*, 4 (2010) 160–177.

30. H. Singh, K. Jamie, M. Animesh, *Waste and Biomass Valorization*, 9 (2018) 1181–1189.
31. M.T. Reza, W. Yan, M.H. Uddin, J.G. Lynam, S.K. Hoekman, C.J. Coronella, V.R. Vásquez, *Bioresour. Technol.*, 139 (2013) 161–169.
32. T. Wang, Y. Zhai, Y. Zhu, C. Li, G. Zeng, *Renew. Sustain. Energy Rev.*, 90 (2018) 223–247.
33. H.S. Kambo, A. Dutta, *Energy Convers. Manag.*, 105 (2015) 746–755.
34. K. Thirugnanasambandham, V. Sivakumar, *J. Saudi Soc. Agric. Sci.*, 16 (2017) 358–366.
35. P. Loganathan, W.G. Shim, D.P. Sounthararajah, M. Kalaruban, T. Nur, S. Vigneswaran, *Environ. Sci. Pollut. Res.*, 25 (2018) 16664–16675.
36. A.R. Fischer, L. Sgolik, A. Kreller, C. Dornack, *Water*, 10 (2018).
37. O.A. Odubiyi, A.A. Awoyale, A.C. Eloka-Eboka, *Int. J. Environ. Bioenergy*, 2012 (2012) 162–175.
38. M.A. Hossain, H.H. Ngo, W.S. Guo, T. Setiadi, *Bioresour. Technol.*, 121 (2012) 386–395.
39. R. Asadi, H. Abdollahi, M. Gharabaghi, Z. Boroumand, *Adv. Powder Technol.*, 31 (2020) 1480–1489.
40. S.K. Kandasamy, K. Kandasamy, *Int. J. Electrochem. Sci.*, 14 (2019) 4718–4729.
41. S.K. Kandasamy, K. Kandasamy, *J. New Mater. Electrochem. Syst.*, 22 (2019) 125–131.
42. W. Zhu, *J. Sport Heal. Sci.*, 5 (2016) 77–79.
43. M. Bousquet-Mélou, A. Jehanne, *J. Comb. Theory. Ser. B*, 96 (2006) 623–672.
44. J. Karch, *Collabra Psychol.*, 6 (2020) 1–11.
45. C.D. Venkatachalam, M. Sengottian, S. Kandasamy, K. Balakrishnan, *Glob. NEST Int. J.*, 21 (2019) 410–421.
46. N. Shi, S. Tang, Y. Liu, L. Chen, H. Zhang, H. Huang, Y. Liu, *Biomass Convers. Biorefinery*, 152 (2021).
47. S. Kannan, I. Burelle, V. Orsat, G.S.V. Raghavan, *Waste and Biomass Valorization*, 11 (2020) 3553–3565.
48. M. Naderi, M. Vesali-Naseh, *Biomass Convers. Biorefinery*, 11 (2021) 1443–1451.
49. I.S. Mohammed, R. Na, K. Kushima, N. Shimizu, *Sustainability*, 12 (2020) 5100.
50. X. Zhang, B. Gao, S. Zhao, P. Wu, L. Han, X. Liu, *J. Clean. Prod.*, 242 (2020) 118426.
51. M. Barbanera, A. Cardarelli, E. Carota, M. Castellini, T. Giannoni, S. Ubertini, *Sci. Rep.*, 11 (2021) 1–16.
52. S.M. Senthil, R. Parameshwaran, S. Ragu Nathan, M. Bhuvanesh Kumar, K. Deepandurai, *Struct. Multidiscip. Optim.*, 62 (2020) 1117–1133.
53. E. Georgiou, M. Mihajlović, J. Petrović, I. Anastopoulos, C. Dosche, I. Pashalidis, D. Kalderis, *Bioresour. Technol.*, 337 (2021) 125458.
54. M. Saber, F. Takahashi, K. Yoshikawa, *Environ. Sci. Pollut. Res.*, 25 (2018) 32721–32734.
55. X. He, T. Zhang, Q. Xue, Y. Zhou, H. Wang, N.S. Bolan, R. Jiang, D.C.W. Tsang, *Sci. Total Environ.*, 778 (2021) 146116.
56. S. Lata, P.K. Singh, S.R. Samadder, *Int. J. Environ. Sci. Technol.*, 12 (2015) 1461–1478.
57. N. Ballav, R. Das, S. Giri, A.M. Muliwa, K. Pillay, A. Maity, *Chem. Eng. J.*, 345 (2018) 621–630.
58. E.C. Umejuru, E. Prabakaran, K. Pillay, *Results Mater.*, 7 (2020) 100117.
59. S.B. Kabakcı, S.S. Baran, *Waste Manag.*, 100 (2019) 259–268.
60. F.M. Jais, C.Y. Chee, Z. Ismail, S. Ibrahim, *J. Environ. Chem. Eng.*, 9 (2021) 104829.
61. F. Li, A.R. Zimmerman, X. Hu, Z. Yu, J. Huang, B. Gao, *Chemosphere*, 254 (2020) 126866.
62. S.L. Chiam, H.N. Lim, S.M. Hafiz, A. Pandikumar, N.M. Huang, *Sci. Rep.*, 8 (2018) 1–7.
63. A. Durairaj, T. Sakthivel, S. Ramanathan, A. Obadiah, S. Vasanthkumar, *Cellulose*, 26 (2019) 3313–3324.
64. F. Wu, T. Zhao, Y. Yao, T. Jiang, B. Wang, M. Wang, *Chemosphere*, 238 (2020) 124638.
65. Y.J. Lee, J.C. Jung, S. Park, J.G. Seo, S.H. Baeck, J.R. Yoon, J. Yi, I.K. Song, *Curr. Appl. Phys.*, 10 (2010) 947–951.

66. P. Hao, X. Ma, J. Xie, F. Lei, L. Li, W. Zhu, X. Cheng, G. Cui, B. Tang, *Sci. China Chem.*, 61 (2018) 797–805.